Thymidylate synthase disruption to limit cell proliferation in cell therapies

Rocio Sartori-Maldonado[1], Hossam Montaser[1], Inkeri Soppa[1], Solja Eurola[1], Melanie Balaz[1], Henri Puttonen[4], Timo Otonkoski[1,2], Jonna Saarimäki-Vire[1], Kirmo Wartiovaara[1,3*].

Affiliations:

1- Stem Cells and Metabolism Research Program, Faculty of Medicine, University of Helsinki, Helsinki, Finland
2- Children's Hospital, University of Helsinki and Helsinki University Hospital, Helsinki, Finland
3- Clinical Genetics, Helsinki University Hospital, Helsinki, Finland
4- Department of Pathology, Helsinki University Hospital, Helsinki, Finland

*Corresponding author: kirmo.wartiovaara@helsiki.fi

Abstract

Engineered cells hold great promise for regenerative medicine and gene therapy. However, living cell products entail a fundamental biological risk of unwanted growth. Here, we describe a novel metabolic safety system to control cell proliferation without added genetic elements. We inactivated a key enzyme for nucleotide metabolism, *TYMS*, in several cell lines, thus obtaining cells that proliferate only when supplemented with exogenous thymidine but fail to replicate in its absence. Under supplementation, *TYMS*$^{-/-}$ pluripotent stem cells proliferate normally, produce teratomas and differentiate into potentially therapeutic cell types such as pancreatic beta cells. After differentiation, the postmitotic cells do not require thymidine to function, as seen by prolonged *in vivo* production of human insulin in implanted mice. Hence, this method allows robust cell culture and manufacture while mitigating the risk of uncontrolled growth of transplanted cells.

One Sentence Summary: Genetic disruption of DNA synthesis prevents unwanted proliferation in cell therapies without affecting cell function.

Introduction

Somatic cell therapies offer new possibilities for previously untreatable or challenging medical conditions. Among the cell types used in such therapies, induced pluripotent stem cells (hiPSCs) have garnered significant attention due to their availability from patient-specific somatic cells (*1*, *2*) and their capability to differentiate into potentially therapeutic cell lineages, such as glucose-responsive insulin secreting pancreatic islets (*3*, *4*). Furthermore, the improved technologies for gene transfer and genome editing enable the development of genetically modified cell-based therapies with enhanced therapeutic potential (*5*–*7*).

The use of hiPSC offers several advantages over mesenchymal and embryonic stem cells (MSC and ESC, respectively). HiPSCs circumvent ethical concerns associated with the embryo derived ESCs (*8*, *9*). Unlike donor-derived MSCs and ESCs, hiPSCs' patient-specificity minimizes the risk of immune rejection and graft-versus-host disease (*10*, *11*). Moreover, stem cells can be further genetically modified by silencing or modifying genes involved *e.g.* in immune recognition (*12*) . These features broaden their applications in disease modeling and therapy development, and may enhance their compatibility for allogeneic cell therapies, reducing the need for immunosuppression compared to other cell sources. However, although the universal off-the-shelf cell products decrease the risk for immune rejection, this diminished immunogenicity can also lead to problematic immune evasion and potential oncogenic events.

On top of creating biologically useful cells for a desired clinical purpose, a successful therapeutic product needs to meet the criteria for safety and manufacture scalability. These two goals, however, often compromise each other, since manufacturing benefits from robust cell growth, but intensive or unlimited proliferation poses a threat when the cells are transferred to patients (*13*, *14*). Attempts to create safer cells for therapy have yielded different strategies (*15*, *16*). These safety systems aim to prevent uncontrolled proliferation or selectively eliminate the transplanted cells if necessary (*17*, *18*). Some of the existing safety strategies include the use of inducible apoptotic systems, suicide genes, antibody-mediated cell depletion, and gene editing-based switches (Table 1). Often, these switches work by reversibly activating or inactivating genes upon exposure to a small molecule (ON- and OFF-switches, respectively). However, they all present remarkable challenges: susceptibility to genetic silencing or alteration, transgenic or viral-derived origin, slow activation speed, rapid remission and/or potential neurotoxicity (*16*, *19*, *20*).

62 In this context, we envisioned the generation of an *endogenous* safety strategy by disrupting
63 a key metabolic gene, whose function can be compensated by administering an easily available
64 compound. Using CRISPR-Cas9, we genetically inactivated thymidylate synthase (*TYMS*), the
65 only known enzyme in charge of the *de novo* thymidylate (dTMP) synthesis (***21***). This knock-
66 out generates rescuable auxotrophy towards thymidine and restricts the synthesis of DNA,
67 without altering normal RNA or protein production (Fig. 1.A). This means that dividing cells
68 depend on external supplementation of thymidine to proliferate and achieve robust
69 manufacturing of the cells of interest. However, once the cells have exited the cell cycle and
70 terminally differentiated, they do not require supplementation to synthesize nucleic acids.
71 While preventing dividing cells from proliferating uncontrollably, this approach does not
72 require the use of small molecules nor the insertion of large transgenic elements. Hence, it
73 cannot be silenced by mutagenesis, and it does not result leaky or immunogenic.
74 Our results provide evidence that the culture and proliferation of *TYMS*$^{-/-}$ cells can be
75 regulated with exogenous dTMP *in vitro* and *in vivo*. Furthermore, the characterization and
76 differentiation of *TYMS*$^{-/-}$-hiPSC show that they provide a functional source for cell therapy that
77 does not sustain unwanted proliferation without external dTMP supplementation.
78

79 ## Results

80 ### Disruption of *TYMS* makes proliferative cells dependent on thymidine supplementation

81 The human thymidylate synthase (PDB: 5X5D) is evolutionarily highly conserved. The
82 functional enzymatic ligand pocket is encoded by exons 4 (amino acid R175), 5 (P193, C195,
83 Q214, S216, D218, R225) and 6 (H256, Y258) ***(22)***. Therefore, to disrupt TYMS activity, we deleted
84 the exon 5 with a dual sgRNA Cas9 knock-out approach targeting both intron 4 and intron 5. (Fig.
85 1.B). This removed the enzyme´s active site, generated an early stop codon in exon 6 and
86 depleted the enzyme expression at both mRNA and protein levels (Fig. 1.C-D, Fig. S1.A-B) in
87 several immortal cell lines.
88

89 We hypothesized that *TYMS*$^{-/-}$ cells could be cultured and manufactured normally with
90 external dTMP supplementation, but they would cease to proliferate in its absence. Therefore,
91 we followed the growth of *TYMS*$^{-/-}$-hiPSC (HEL24.3) (***23***) and cancer cell lines without or with
92 dTMP supplementation (25 µM). The untreated (*TYMS*$^{+/+}$) cell lines were used as controls. The

93 results suggest that *TYMS*$^{-/-}$ cells proliferate at a rate comparable to *TYMS*$^{+/+}$ when supplemented
94 with thymidine, while the proliferation capacity of non-supplemented *TYMS*$^{-/-}$ cells was
95 drastically impaired (Fig. 1.E). To determine the optimal concentration of dTMP for culturing
96 TYMS$^{-/-}$-hiPSC, we run a dose-dependent assay using a range of 0.3 uM to 5 mM exogenous dTMP
97 to explore their tolerance limits (Fig. 1.F and Fig. S1.C). Contrarily to *TYMS*$^{+/+}$ lines, *TYMS*$^{-/-}$-hiPSCs
98 could not sustain growth at physiological concentrations of thymidine (reference: 0.5-1.4 µM)
99 (*24*). Cell cycle analysis by flow cytometry of *TYMS*$^{-/-}$-hiPSC cells reveal that in the first 24 h of
100 dTMP withdrawal, the cells accumulate in G0-G1 and S-phase, and then, as they should continue
101 to G2, accumulate in the subG0-G1 phase (Fig. 1G and Fig. S1.D). On the other end of this
102 spectrum, we observe shift in the cytotoxic threshold at higher concentrations; while the growth
103 rate of *TYMS*$^{+/+}$-cells decreases at concentrations higher than 200 µM, knock-out cells suffer
104 comparable cytotoxic effects at concentrations higher than 1 mM (1000 µM) (Fig. 1.F).
105 In summary, our results show that *TYMS*$^{-/-}$ cells grow normally and can be expanded
106 extensively under dTMP supplementation. Thymidine withdrawal, however, stalls cells in S phase
107 and inhibits progression to G2/M, likely due to replicative stress from nucleotide imbalance.
108
109 ### *TYMS* knock-out hiPSCs maintain pluripotency and genomic integrity
110 The *TYMS*$^{-/-}$-hiPS cell lines performed equally well on standard pluripotency analysis as their
111 non-edited counterparts. They showed positive staining for pluripotency markers NANOG, OCT4,
112 SOX2 and SSEA4 and comparable mRNA expression of *SOX2, NANOG* and *OCT4* to *TYMS*$^{+/+}$-hiPSC
113 (Fig. 1.G and Fig. S1.E). Furthermore, their chromosomal integrity remained unaltered by the
114 editing process in prolonged culture, tested in several time points for up to 25 passages (Fig.
115 S1.F). The differentiation into the three germ layers with or without dTMP supplementation
116 revealed that the cells successfully differentiate into ectoderm, mesoderm and endoderm when
117 supplemented with dTMP at the early stages of differentiation (Fig. 2.A, C). Lack of
118 supplementation from the *TYMS*$^{-/-}$ cells during d0-d14 produced significantly less embryoid
119 bodies at d14 (Fig. 2.B). By day 28, however, all attached cells from supplemented and non-
120 supplemented cells expressed characteristic markers of the three germ layers (Fig 2.C, Fig. S1.G).
121
122

123 Thymidine deficiency drastically reduces proliferation and teratoma formation in mice
124 transplanted with TYMS$^{-/-}$-hiPSCs

125 Next, we aimed to translate the *in vitro* trilineage differentiation to an *in vivo* setting. We
126 implanted undifferentiated TYMS$^{+/+}$- and TYMS$^{-/-}$-hiPSC aggregates subcutaneously in mice,
127 without or with 100 mg/kg/day dTMP supplementation in the drinking water (Fig. 2.D). After 6
128 weeks, we retrieved the teratomas from the euthanized mice and analyzed their size,
129 composition, and proliferation (Fig. 2.E-K).

130 *TYMS*$^{+/+}$-hiPSC produced teratoma-like growth in all mice regardless of the thymidine
131 supplementation, while *TYMS*$^{-/-}$-hiPSC produced visible teratomas only under dTMP
132 supplementation. Only one mouse presented a small *TYMS*$^{-/-}$-derived teratoma without
133 supplementation (Fig. 2.E). Histological analysis and immunocytochemistry showed that *TYMS*$^{+/+}$-
134 hiPSC generated dense teratomas with higher cellularity (Fig. 2.F-G). Contrarily, *TYMS*$^{-/-}$-hiPSC
135 overall produced low-density teratomas. As expected, immunohistochemical analysis of *TYMS*$^{-/-}$
136 -hiPSC derived tumors resulted negative for TYMS, while *TYMS*$^{+/+}$-hiPSCs present a rather
137 homogenous expression of the protein (Fig. 2.H). Additionally, analogous to the *in vitro*
138 experiment, we could identify regions expressing markers for the three germ layers (Fig. 2.I) in
139 all analyzed tumors. Importantly, the absence of thymidine supplementation resulted in
140 significantly less proliferative tumors with low cellularity, (Fig. 2.J-K), and composed mainly of
141 primitive glial, epithelial, and mesenchymal tissue.

142

143 Non-supplemented TYMS$^{-/-}$-hiPSC differentiate into functional beta cells *in vitro*

144 One promising target for cell replacement therapy is diabetes, in which stem cell derived
145 insulin-producing beta cells act as the therapeutic source of insulin. We evaluated the safety,
146 quality, and function of *TYMS*$^{-/-}$-hiPSC-derived pancreatic islets using a well-defined, multi-step
147 protocol for beta cell differentiation (Fig. 3.A) (***3***, ***4***). We differentiated *TYMS*$^{-/-}$ -hiPSCs (HEL24.3)
148 *in vitro*, supplemented with thymidine (40 µM) through the whole differentiation experiment.
149 Meanwhile, as expected, non-supplemented *TYMS*$^{-/-}$ cells did not survive thymidine withdrawal
150 at early stages of differentiation, making further characterization of this condition impossible.
151 Non-supplemented *TYMS*$^{+/+}$-hiPSC were used as controls. We did not observe differences
152 between *TYMS*$^{+/+}$-hiPSC differentiated with or without dTMP supplementation, suggesting that

153 the addition of dTMP at our working concentrations (up to 40 µM) does not affect *TYMS*$^{+/+}$-cells
154 (data not shown). Hereafter, we did not supplement *TYMS*$^{+/+}$-hiPSC during the differentiation.
155 We evaluated the progression of the differentiation by flow cytometry, RT-qPCR, and
156 immunocytochemical analysis of cell identity markers at several developmental stages. *TYMS*$^{+/+}$-
157 and supplemented *TYMS*$^{-/-}$-hiPS cells showed comparable *in vitro* expression levels of markers at
158 the definitive endoderm (DE) stage (CXCR4), pancreatic endocrine progenitor stage (S4) (PDX1,
159 NKX6.1) and endocrine maturation stage (S7) (insulin – INS, glucagon – GCG, NKX6.1, PDX1, C-
160 peptide) by flow cytometry and immunocytochemistry (Fig. 3.B and Fig. S2.A-C). In
161 transcriptomic analysis by RT-qPCR, we found that both the *TYMS*$^{-/-}$- and *TYMS*$^{+/+}$- derived islets
162 expressed similar levels of markers at stages DE and S4 stages, and markers of mature beta-cells
163 at week 4 of stage 7 (S7W4) (Fig. 3.C). *TYMS*$^{-/-}$- derived islets presented lower *TYMS* mRNA levels
164 that their *TYMS*$^{+/+}$ counterparts. Hereafter, we withdrew dTMP supplementation from the islets
165 cultured for *in vivo* implantation. By the last stage before implantation (S7W4), the *TYMS*$^{-/-}$-hiPSC
166 islets showed normal morphology and standard percentage of insulin, glucagon, synaptophysin
167 (SYP) and SLC18A1 expressing cells (Fig. 3.D-E), while displaying a significantly decreased
168 proliferative index by KI67 analysis (Fig. 3.F). Accordingly, *TYMS*$^{-/-}$ and *TYMS*$^{+/+}$ hiPSC-derived islets
169 showed similar *in vitro* levels of glucose-, exendin 4- and KCl- induced functional insulin secretion
170 at S7W4 (Fig. 4.G-E) and even after 3 months in culture (S7W16, Fig. 3.I). Thus, these results
171 overall indicate that *TYMS*$^{-/-}$-hiPSC lines efficiently differentiate to functional SC-islets,
172 comparable to their control counterparts, while displaying reduced proliferation upon dTMP
173 withdrawal.
174

175 ### *TYMS*$^{-/-}$-hiPSC derived beta cells without dTMP supplementation efficiently regulate
176 ### blood glucose *in vivo*

177 We next evaluated the function of mature *TYMS*$^{-/-}$ beta cells (S7) *in vivo* by engrafting them
178 under the kidney capsule of immunosuppressed mice without dTMP supplementation (Fig. 4.A).
179 We implanted mice with *TYMS*$^{+/+}$- or *TYMS*$^{-/-}$-hiPSC -derived islets, and monitored their body
180 weight, glucose levels and the grafts' production of human C-peptide for three months.
181 Both *TYMS*$^{-/-}$ and *TYMS*$^{+/+}$ control islet produced comparable levels of human C-peptide and
182 lowered the mouse blood glucose (Fig. 4.B-C). All mice maintained their normal body weights
183 (Fig. S2.F) and did not show any other signs of health concerns.

184 Three months post-implantation, we performed an insulin tolerance test by treating the mice
185 with insulin to test the ability of the grafts to shut down their *bona fide* insulin secretion in
186 response to low glucose levels. Upon the decline of circulating glucose levels in response to the
187 exogenously injected insulin (Fig. 4.D), our *TYMS*$^{-/-}$ grafts stopped their insulin secretion at
188 comparable rates as their *TYMS*$^{+/+}$ counterparts, suggesting an appropriate regulation of this
189 process (Fig. 4.E-F).

190 Immunohistochemistry on the implanted grafts showed comparable percentage of insulin and
191 glucagon producing cells in *TYMS*$^{+/+}$ and *TYMS*$^{-/-}$ grafts at 1- and 3-months post-implantation (Fig.
192 4.G-H).

193 Additionally, to quantify the proliferation of the cells in the grafts *in vivo* through time (1 and
194 3 months), we ran immunohistochemical analysis against KI67 and we supplemented the
195 drinking water of the mice with EdU for 5 days before euthanizing them. Interestingly, despite
196 the significant reduction on active proliferation in *TYMS*$^{-/-}$ cells (by KI67 expression analysis), the
197 uptake of EdU did not differ significantly (Fig. 4.I-L and Fig. S3.D-E), possibly due to the uptake of
198 EdU as a source of thymidine.

199 To summarize, we demonstrate here that *TYMS*$^{-/-}$-hiPSCs differentiate into pancreatic beta
200 cells and function normally *in vitro* and *in vivo*, as seen by prolonged regulated human insulin
201 secretion.

202

203 ## Discussion

204

205 We have developed a method to generate controllable cells without inserting any external
206 genetic elements. By disrupting the rate-limiting DNA-specific nucleotide synthesis reaction,
207 we have obtained cells auxotrophic to thymidine. This novel safety mechanism allows *TYMS*$^{-/-}$-
208 hiPSCs to expand as needed for undefined periods showing no signs of exhaustion, but only
209 when externally supplemented with thymidine. In its absence, contrarily, the cells fail to
210 proliferate. Moreover, this method does not affect function of the therapeutic differentiated
211 cells *in vitro* or *in vivo*.

212 The *TYMS*$^{-/-}$ -hiPSCs retain their pluripotency and differentiate successfully into different cell
213 types. Non-supplemented *TYMS*$^{-/-}$-hiPSC generate small or no teratomas *in vivo* with a
214 significantly lower proliferative index (KI67), pointing to the loss of proliferative capacity of
215 these cells under physiological concentrations of thymidine. Previous reports by Diehl et al (*25*)

216 suggest that thymidine withdrawal from *TYMS*$^{-/-}$ hiPSCs leads to replicative stress and cell cycle
217 arrest from nucleotide starvation. Supported by the results of our cell cycle analysis, we
218 hypothesize that cells that have not exited the cell cycle die likely soon after this replicative
219 stress is sensed, at the S-G2 checkpoint (*25*, *26*). However, we observed an extended survival
220 time of non-supplemented *TYMS*$^{-/-}$ cells when they form 3D aggregates both in *in vitro* and *in*
221 *vivo* differentiation experiments (embryoid bodies and teratoma formation, respectively). As
222 TYMS activity is required for the synthesis of DNA but not that of RNA, this may suggest the
223 recycling of thymidine from apoptotic cells until cell cycle exit (*27*). Once they exit the cell cycle,
224 the cells may survive as differentiated cells for extended periods. Accordingly, we see no
225 functional alterations in the terminally differentiated cells without dTMP supplementation *in*
226 *vitro* or *in vivo*. The hiPSC-derived pancreatic islets survived implantation and proved to
227 successfully secrete human insulin and lower blood glucose up to the measured three months
228 after implantation, without affecting the overall wellbeing of the mice.

229 The advances in basic science and technological developments simultaneously aid and
230 pressure pre-clinical studies in their translation to clinical applications. On one hand, improved
231 gene and cell manipulation protocols have increased the efficiency and widen the application
232 of somatic-cell and gene therapies, tissue-engineered medicines, and CRISPR-based products.
233 On the other hand, the safety concerns arising from altering DNA challenge further clinical
234 applications. Hence, strategies to make cellular products safer become a need. Ideally, a safety
235 mechanism for cell therapies selectively targets cells that retain or have acquired the ability for
236 dangerous proliferation, without affecting the functional therapeutic cells. Although attempts
237 to control the activity and proliferation of the therapeutic cells have proven relatively efficient,
238 they present some inherent disadvantages. As most *safety switches* alter DNA by including
239 exogenous genetic material, they often result complex, immunogenic or susceptible to
240 mutations or silencing, ultimately affecting the partial/remissive function of the system (*20*).

241 In this regard, we believe our system brings added value to the efficiency and versatility of
242 safety mechanisms. By a simple genetic manipulation of endogenous DNA, we generated cells
243 auxotrophic towards thymidine. This approach not only evades the insertion of external
244 genetic sequences, but additionally allows for control of cellular proliferation by addition of a
245 simple, FDA-approved compound (thymidine). Thus, it facilitates the mass expansion and
246 generation of therapeutic cells, that lose their proliferative capacity, but not their function,

247 under *in vivo* concentrations of thymidine. Moreover, *in vivo* thymidine administration may
248 control the function and efficiency of some therapeutic cells, such as immunotherapies,
249 expanding the applications of this strategy.

250 The genetic disruption applied in this research brings about an additional advantage: the
251 use of the *TYMS* locus as a genomic *safe harbor*. This opens the doors to future additions and
252 combinatory developments with other selection and safety systems. We see this versatile
253 feature as a solution to current limitations and an aid to expand the applications of *TYMS*
254 disruption to other aims and other therapeutic cell types. We expect the replication and
255 utilization of these results to contribute to the optimization of hiPSC-derived and other cellular
256 products, and to the future development of safer efficient cell-based therapies.

257
258

259 ## References

260 1. K. Takahashi, S. Yamanaka, Induction of Pluripotent Stem Cells from Mouse Embryonic
261 and Adult Fibroblast Cultures by Defined Factors. Cell. 126(2006), doi:
262 10.1016/j.cell.2006.07.024.
263 2. J. Weltner, D. Balboa, S. Katayama, M. Bespalov, K. Krjutškov, E. M. Jouhilahti, R.
264 Trokovic, J. Kere, T. Otonkoski, Human pluripotent reprogramming with CRISPR
265 activators. Nat Commun. 9 (2018), doi:10.1038/s41467-018-05067-x.
266 3. T. Barsby, H. Ibrahim, V. Lithovius, H. Montaser, D. Balboa, E. Vähäkangas, V. Chandra,
267 J. Saarimäki-Vire, T. Otonkoski. Differentiating functional human islet-like aggregates
268 from pluripotent stem cells. STAR Protocols. 3 (2022), doi: 10.1016/j.xpro.2022.101711.
269 4. D. Balboa, T. Barsby, V. Lithovius, J. Saarimäki-Vire, M. Omar-Hmeadi, O. Dyachok, H.
270 Montaser, P.E. Lund, M. Yang, H. Ibrahim, A. Näätänen, V. Chandra, H. Vihinen, E.
271 Jokitalo, J. Kvist, J. Ustinov, A.I. Nieminen, E. Kuuluvainen, V. Hietakangas, P. Katajisto, J.
272 Lau, P.O. Carlsson, S. Barg, A. Tengholm & T. Otonkoski. Functional, metabolic and
273 transcriptional maturation of human pancreatic islets derived from stem cells. Nat
274 Biotechnol. 40 (2022), doi:10.1038/s41587-022-01219-z.
275 5. R. Maldonado, S. Jalil, K. Wartiovaara, Curative gene therapies for rare diseases. J
276 Community Genet. 12 (2020), doi:10.1007/s12687-020-00480-6.
277 6. M. L. Maeder, C. A. Gersbach. Genome-editing Technologies for Gene and Cell Therapy.
278 Mol. Therapy. 24 (2016), doi:10.1038/mt.2016.10.
279 7. P. D. Hsu, E. S. Lander, F. Zhang, Development and applications of CRISPR-Cas9 for
280 genome engineering. Cell. 157 (2014), doi: 10.1016/j.cell.2014.05.010.
281 8. A. Picken, J. Harriman, A. Iftimia-Mander, L. Johnson, A. Prosser, R. Quirk, R. Thomas, A
282 Monte Carlo framework for managing biological variability in manufacture of autologous
283 cell therapy from mesenchymal stromal cells therapies. Cytotherapy. 22, (2020). doi:
284 10.1016/j.jcyt.2020.01.006.
285 9. M.A.M. Aboul-Soud, A. J. Alzahrani, A. Mahmoud. Induced Pluripotent Stem Cells
286 (iPSCs)-Roles in Regenerative Therapies, Disease Modelling and Drug Screening. Cells 10
287 (2021), doi:10.3390/cells10092319.

10. T. Zhao, Z.-N. Zhang, Z. Rong, Y. Xu, Immunogenicity of induced pluripotent stem cells Nature, 474 (2011), doi:10.1038/nature10135.
11. M. Themeli, C. C. Kloss, G. Ciriello, V. D. Fedorov, F. Perna, M. Gonen, M. Sadelain, Generation of tumor-targeted human T lymphocytes from induced pluripotent stem cells for cancer therapy. Nat. Biotechnology. 31 (2013), doi:10.1038/nbt.2678.
12. H. Xu, B. Wang, M. Ono, A. Kagita, K. Fujii, N. Sasakawa, T. Ueda, P. Gee, M. Nishikawa, M. Nomura, F. Kitaoka, T. Takahashi, K. Okita, Y. Yoshida, S. Kaneko, A. Hotta, Targeted Disruption of HLA Genes via CRISPR-Cas9 Generates iPSCs with Enhanced Immune Compatibility. Cell Stem Cell. 24 (2019). doi: 10.1016/j.stem.2019.02.005.
13. A. S. Lee, C. Tang, F. Cao, X. Xie, K. Van Der Bogt, A. Hwang, A. J. Connolly, R. C. Robbins, J. C. Wu, Effects of cell number on teratoma formation by human embryonic stem cells. Cell Cycle. 8 (2009). doi: 10.4161/cc.8.16.9353.
14. H. Hentze, P. L. Soong, S. T. Wang, B. W. Phillips, T. C. Putti, N. R. Dunn, Teratoma formation by human embryonic stem cells: Evaluation of essential parameters for future safety studies. Stem Cell Res. 3 (2009), doi:10.1016/j.scr.2009.02.002.
15. V. Wiebking, J. O. Patterson, R. Martin, M. K. Chanda, C. M. Lee, W. Srifa, G. Bao, M. H. Porteus, Metabolic engineering generates a transgene-free safety switch for cell therapy. Nat. Biotechnology, 38 (2020), doi:10.1038/s41587-020-0580-6.
16. C. L. Bonifant, H. J. Jackson, R. J. Brentjens, K. J. Curran, Toxicity and management in CAR T-cell therapy. Mol Ther Oncolytics. 3, (2016). doi: 10.1038/mto.2016.11.
17. T.-T. Lim, C. Geisen, M. Hesse, B. K. Fleischmann, K. Zimmermann, Lentiviral Vector Mediated Thymidine Kinase Expression in Pluripotent Stem Cells Enables Removal of Tumorigenic Cells) Lentiviral Vector Mediated Thymidine Kinase Expression in Pluripotent Stem Cells Enables Removal of Tumorigenic Cells. PLoS One. 8 (2013), doi: 10.1371/journal.pone.0070543.
18. F. Chen, B. Cai, Y. Gao, X. Yuan, F. Cheng, T. Wang, M. Jiang, Y. Zhou, B. T. Lahn, W. Li, A. P. Xiang, Suicide gene-mediated ablation of tumor-initiating mouse pluripotent stem cells. Biomaterials 34 (2013), doi:10.1016/j.biomaterials.2012.11.018.
19. V. Volarevic, B. Simovic Markovic, M. Gazdic, A. Volarevic, N. Jovicic, N. Arsenijevic, L. Armstrong, V. Djonov, M. Lako, M. Stojkovic, Ethical and Safety Issues of Stem Cell-Based Therapy. Int. J. Med. Sci. 15 (2018), doi: 10.7150/ijms.21666.
20. A. C. Sahillioglu, T. N. Schumacher, Safety switches for adoptive cell therapy. Curr Opin Immunol. 74 (2022), 10.1016/j.coi.2021.07.002.
21. D. D. Anderson, C. M. Quintero, P. J. Stovera, Identification of a de novo thymidylate biosynthesis pathway in mammalian mitochondria. Proc Natl Acad Sci U S A. 108, (2011), doi: 10.1073/pnas.1103623108.
22. D. Chen, A. Jansson, D. Sim, A. Larsson, P. Nordlund, Structural analyses of human thymidylate synthase reveal a site that may control conformational switching between active and inactive states. J Biol Chem. 292, (2017), doi: 10.1074/jbc.M117.787267.
23. R. Trokovic, J. Weltner, T. Otonkoski, Generation of iPSC line HEL24.3 from human neonatal foreskin fibroblasts. Stem Cell Res. 15 (2015), doi: 10.1016/j.scr.2015.05.012.
24. T. W. Traut, Physiological concentrations of purines and pyrimidines. Mol Cell Biochem. 140 (1994). doi: 10.1007/BF00928361.
25. F. F. Diehl, T. P. Miettinen, R. Elbashir, C. S. Nabel, A. M. Darnell, B. T. Do, S. R. Manalis, C. A. Lewis, M. G. Vander Heiden, Nucleotide imbalance decouples cell growth from cell proliferation. Nat Cell Biol, 24 (2022), doi:10.1038/s41556-022-00965-1.

26. J. C. Saldivar, S. Hamperl, M. J. Bocek, M. Chung, T. E. Bass, F. Cisneros-Soberanis, K. Samejima, L. Xie, J. R. Paulson, W. C. Earnshaw, D. Cortez, T. Meyer, K. A. Cimprich, An intrinsic S/G2 checkpoint enforced by ATR. Science. 361, (2018), doi: 10.1126/science.aap9346.
27. C. K. Brock, S. T. Wallin, O. E. Ruiz, K. M. Samms, A. Mandal, E. A. Sumner, G. T. Eisenhoffer, Stem cell proliferation is induced by apoptotic bodies from dying cells during epithelial tissue maintenance, doi:10.1038/s41467-019-09010-6.
28. J. P. Concordet, M. Haeussler, CRISPOR: Intuitive guide selection for CRISPR/Cas9 genome editing experiments and screens. Nucleic Acids Res (2018), doi: 10.1093/nar/gky354.
29. J. Schindelin, I. Arganda-Carreras, E. Frise, V. Kaynig, M. Longair, T. Pietzsch, S. Preibisch, C. Rueden, S. Saalfeld, B. Schmid, J. Y. Tinevez, D. J. White, V. Hartenstein, K. Eliceiri, P. Tomancak, A. Cardona, Fiji: an open-source platform for biological-image analysis. Nature Methods. 9 (2012), https://doi.org/10.1038/nmeth.2019.
30. D. R. Stirling, M. J. Swain-Bowden, A. M. Lucas, A. E. Carpenter, B. A. Cimini, A. Goodman, CellProfiler 4: improvements in speed, utility and usability. BMC Bioinformatics. 22 (2021), https://doi.org/10.1186/s12859-021-04344-9.
31. V. Lithovius, J. Saarimäki-Vire, D. Balboa, H. Ibrahim, H. Montaser, T. Barsby, T. Otonkoski, SUR1-mutant iPS cell-derived islets recapitulate the pathophysiology of congenital hyperinsulinism. Diabetologia. 64, (2021), doi: 10.1007/s00125-020-05346-7.
32. Z. Karjoo, X. Chen, A. Hatefi, Progress and Problems with the Use of Suicide Genes for Targeted Cancer Therapy. Adv Drug Deliv Rev. 99 (2016), doi: 10.1016/j.addr.2015.05.009.
33. C. Berger, M. E. Flowers, E. H. Warren, S. R. Riddell, Analysis of transgene-specific immune responses that limit the in vivo persistence of adoptively transferred HSV-TK–modified donor T cells after allogeneic hematopoietic cell transplantation. Blood. 107 (2006), doi: 10.1182/blood-2005-08-3503.
34. S. Sheikh, D. Ernst, A. Keating, Prodrugs and prodrug-activated systems in gene therapy. Mol. Therapy. 29 (2021), doi:10.1016/j.ymthe.2021.04.006.
35. B. A. Buil, C. Tackenberg, R. Rust, Editing a gateway for cell therapy across the blood–brain barrier. Brain. 146 (2023), doi: 10.1093/brain/awac393.
36. S. Pellegrini, V. Zamarian, V. Sordi, Strategies to Improve the Safety of iPSC-Derived β Cells for β Cell Replacement in Diabetes. Transpl Int., 35 (2022), doi: 10.3389/ti.2022.10575.
37. P. Tiberghien, C. W. Reynolds, J. Keller, S. Spence, M. Deschaseaux, J.-M. Certoux, E. Contassot, W. J. Murphy, R. Lyons, Y. Chiang, P. Herve, D. L. Longo, F. W. Ruscetti, Ganciclovir treatment of herpes simplex thymidine kinase-transduced primary T lymphocytes: an approach for specific in vivo donor T-cell depletion after bone marrow transplantation?. Blood. 84, (1994). PMID: 8049449.
38. Q. Liang, C. Monetti, M. V. Shutova, E. J. Neely, S. Hacibekiroglu, H. Yang, C. Kim, P. Zhang, C. Li, K. Nagy, M. Mileikovsky, I. Gyongy, H. K. Sung, A. Nagy, Linking a cell-division gene and a suicide gene to define and improve cell therapy safety. Nature. 563 (2018), doi: 10.1038/s41586-018-0733-7.
39. E. A. Austin, B. E. Huber, A first step in the development of gene therapy for colorectal carcinoma: cloning, sequencing, and expression of Escherichia coli cytosine deaminase. Mol Pharmacol. 43 (1993), PMID: 8450832.

40. R. N. Felmer, J. A. Clark, The gene suicide system NTR/CB1954 causes ablation of differentiated 3T3L1 adipocytes by apoptosis. Biol Res. 37 (2004), doi: 10.4067/s0716-97602004000300009.
41. V. K. Gadi, S. D. Alexander, J. E. Kudlow, P. Allan, W. B. Parker, E. J. Sorscher, In vivo sensitization of ovarian tumors to chemotherapy by expression of E. coli purine nucleoside phosphorylase in a small fraction of cells. Gene Ther. 7 (2000), doi: 10.1038/sj.gt.3301286.
42. T. Sato, A. Neschadim, M. Konrad, D. H. Fowler, A. Lavie, J. A. Medin, Engineered Human tmpk/AZT As a Novel Enzyme/Prodrug Axis for Suicide Gene Therapy. Molecular Therapy. 15 (2007), doi: 10.1038/mt.sj.6300122.
43. M. Serafini, M. Manganini, G. Borleri, M. Bonamino, L. Imberti, A. Biondi, J. Golay, A. Rambaldi, M. Introna, Characterization of CD20-transduced T lymphocytes as an alternative suicide gene therapy approach for the treatment of graft-versus-host disease. Hum Gene Ther. 15 (2004), doi: 10.1089/10430340460732463.
44. X. Wang, W. C. Chang, C. L. W. Wong, D. Colcher, M. Sherman, J. R. Ostberg, S. J. Forman, S. R. Riddell, M. C. Jensen, A transgene-encoded cell surface polypeptide for selection, in vivo tracking, and ablation of engineered cells. Blood. 118 (2011).
45. E. Kieback, J. Charo, D. Sommermeyer, T. Blankenstein, W. Uckert, A safeguard eliminates T cell receptor gene-modified autoreactive T cells after adoptive transfer. Proc Natl Acad Sci U S A. 105, 623–628 (2008), doi: 10.1182/blood-2011-02-337360.
46. M. J. Birrer, K. N. Moore, I. Betella, R. C. Bates, Antibody-Drug Conjugate-Based Therapeutics: State of the Science. J Natl Cancer Inst. 111 (2019), doi: 10.1093/jnci/djz035.
47. K. C. Straathof, M. A. Pulè, P. Yotnda, G. Dotti, E. F. Vanin, M. K. Brenner, H. E. Heslop, D. M. Spencer, C. M. Rooney, An inducible caspase 9 safety switch for T-cell therapy. Blood. 105 (2005), doi: 10.1182/blood-2004-11-4564.
48. Y. Liu, Y. Yang, Y. Suo, C. Li, M. Chen, S. Zheng, H. Li, C. Tang, N. Fan, T. Lan, J. Zhou, Y. Li, J. Wang, H. Chen, Q. Zou, L. Lai, Inducible caspase-9 suicide gene under control of endogenous oct4 to safeguard mouse and human pluripotent stem cell therapy. Mol Ther Methods Clin Dev. 24 (2022). doi: 10.1016/j.omtm.2022.01.014.
49. S. Wunderlich, A. Haase, S. Merkert, K. Jahn, M. Deest, H. Frieling, S. Glage, W. Korte, A. Martens, A. Kirschning, A. Zeug, E. Ponimaskin, G. Göhring, M. Ackermann, N. Lachmann, T. Moritz, R. Zweigerdt, U. Martin, Targeted biallelic integration of an inducible Caspase 9 suicide gene in iPSCs for safer therapies. Mol Ther Methods Clin Dev. 26 (2022), https://doi.org/10.1016/j.omtm.2022.05.011.

Aknowledgements

We thank MD Vaino Lithovius and MSc. Nidhi Madhusudan for assistance in image analysis, MSc. Sami Jalil, PhD. Diego Balboa and PhD. Juan Cruz Landoni for scientific discussion and support, MSc. Hazem Ibrahim and MSc. Eliisa Vahankangas for assistance with animal experiments. We thank the Flow cytometry Unit and the Animal facility at Biomedicum Helsinki for their possible contribution to this study.
We thank Helsinki University Hospital research funding, Foundation for Pediatric research, Paulo Foundation, Signe and Ane Gyllenberg Foundation, Magnus Ehrnrooth Foundation, K.

Albin Johansson Foundation, Ida Montin Foundation, Finnish Red Cross Blood Service Research Fund, Diabetes Foundation for financial support.

Author contributions

Conceptualization: RSM, TO, KW
Methodology: RSM, HM, JSV, KW
Investigation: RSM, HM, SE, IS, MB, JSV.
Visualization: RSM
Formal analysis: RSM
Funding acquisition: RSM, TO, KW
Project administration: RSM, KW
Supervision: TO, JSV, KW
Writing – original draft: RSM, KW
Writing – review & editing: RSM, HM, JSV, HP, TO, KW

Conflict of interest

RSM and KW are marked as inventors in a patent application by the University of Helsinki.

473 ## Materials and methods

474

475 ### Culture of HEK293 FT, A431, A549, HSC3

476 We cultured HEK293, epidermoid carcinoma cell line A431, adenocarcinoma human alveolar
477 basal epithelial cells A549, and human oral squamous carcinoma cell line HSC-3 cells in
478 Dulbecco's modified Eagle's medium (DMEM) containing 10% fetal bovine serum (FBS), 100
479 µg/ml penicillin-streptomycin and 2 mM GlutaMAX (all ThermoFisher Scientific). After *TYMS*
480 knock-out, cell media were additionally supplemented with 5-20µM dTMP (ThermoFisher
481 Scientific). We kept the cell lines at 37 °C and 5% CO2, with media change every other day until
482 splitting with TrypLE select (Gibco). All cell lines tested negative for mycoplasma.

483

484 ### Induced Pluripotent Stem cells culture and characterization

485 Human induced pluripotent stem cell (hiPSC) line HEL24.3was cultured on Matrigel (Corning)
486 coated plates in E8 medium (ThermoFisher Scientific) and split using 0.5 mM EDTA. We kept the
487 cell lines at 37 °C and 5% CO2, with media change every other day. All cell lines tested negative
488 for mycoplasma. After *TYMS* knock-out, cell media were additionally supplemented with 5-20
489 µM dTMP. The karyotyping was carried out by Ambar Anàlisis Mèdiques (Barcelona, Spain) by G-
490 banding. We treated edited (passage 20 and 45) and non-edited (passage 20) hiPSC with
491 colcemid for 4 h, 37°C, 5% CO2 and proceeded to prepare the cells as recommended by the
492 service provider.

493

494 ### Genome editing

495 To knock out exon 5, we designed guide RNA targeting intron 4 (I4) and intron 5 (I5) using
496 online tools (https://benchling.com, CRISPOR (***28***), Table S1). We generated the sgRNA by
497 incubating 5 min at 95 °C our gRNA (customized Alt-R CRISPR-Cas9 gRNA, iDT) with Alt-R® CRISPR-
498 Cas9 tracrRNA, ATTO™ 550 (iDT).

499 For each stem cell electroporation experiment, we dissociated 2x10^6 cells into single-cells
500 with StemPro Accutase (ThermoFisher Scientific). We complexed the sgAlt-R® S.p. HiFi Cas9
501 Nuclease V3 and and both sgRNA to form the functional ribonucleoprotein (RNP) and delivered
502 this RNP into the cells, along the Alt-R® Cas9 electroporation enhancer (all from integrated DNA
503 Technologies – iDT), by electroporation with Neon transfection systems (1100 V, 20 ms, 2

504 pulses). Cells were plated onto Matrigel-coated plates containing E8 with 5 µM ROCK inhibitor
505 (Y-27632, Selleckchem) and 20-40 µM dTMP, and incubated at 37 ˚C, 5% CO2.
506 For electroporation experiment with cell lines HSC-3 and A549, A431, cells were dissociated
507 into single cells with TrypLE. SgRNAs were prepared as previously described and delivered to the
508 cells using Neon transfection systems. For HSC3 and A549, the electroporation settings were
509 1250 V, 10 ms, 1 pulse, while for A431 we used 1450 V, 20 ms, 2 pulses. After tranfection, the
510 cells were plated onto plates containing culture media (10% FBS in DMEM) supplemented with
511 20-40 µM dTMP, and incubated at 37 ˚C, 5% CO2.
512 24-48 h after electroporation, we single cell sorted ATTO550 positive cells for monoclonal
513 expansion in 96-well plates containing their corresponding dTMP-supplemented culture media
514 (hiPSC additionally supplemented with 10% Clone R (StemCell Technologies)). The media was
515 refreshed every 72 h until splitting. We individually screened monoclonal colonies by PCR. All
516 PCR products of the selected edited clones were validated by Sanger sequencing, along with the
517 integrity of the top-7 off target sequences (Table S2).
518
519 Embryoid body differentiation
520 To test the pluripotency for an embryonal lineage differentiation, we grew the cells until 90-
521 100% confluency and performed embryoid body (EB) differentiation assay as previously
522 described (*2*). Final plated EBs were fixed with 4%PFA-PBS and analyzed by
523 immunocytochemistry for characteristic markers of the three germ-layers (see list below).
524
525 Teratoma assay
526 Knock-out and wild-type HEL24.3 cells were cultured in ultra-low attachment plates with E8
527 supplemented with 5 µM ROCK inhibitor for 24-48 h to form aggregates. The medium for knock-
528 out cells was additionally supplemented with 40 µM dTMP until 2 h before implantation. Groups
529 of approximately 500 spheres were collected in syringe cannulas for subcutaneous implantation
530 in the legs of the mice. For half of the mice, the drinking water was supplemented with 100
531 mg/kg/day dTMP. 6-8 weeks post implantation the teratomas were extracted and fixed for
532 immunocytochemistry and hematoxilin-eosin stainings as described below.
533

534 dTMP auxotrophy

535 Wild-type and knock-out clones from each cell line were split onto Matrigel coated 6-well
536 plates at a reason of a 25000 cells per well. Each well contained the corresponding medium for
537 the cell line (see *Cell culture*) supplemented with 0 to 5 mM dTMP. Cells were washed and media
538 were refreshed daily to clear away dead cells debris and keep the thymidine concentration as
539 constant as possible.

540

541 Beta-cell differentiation

542 The *in vitro* beta cell differentiation was carried out as previously described (*3*, *4*). Briefly,
543 *TYMS* knock-out and control HEL24.3 hiPS cells were seeded onto Matrigel coated 10 cm plates
544 as previously stated. Differentiation protocol was started 24 h post-seeding, when the medium
545 was changed to D0 medium. Both cell lines were supplemented with 0 or 40 µM dTMP until
546 maturation. At stage 7, dTMP was withdrawn or kept until analysis (weeks 4 to 16 from the first
547 day of S7). The media was refreshed every 2-3 days until analysis.

548

549 Flow cytometry

550 Stage 4 cells and stage 7 stem cell derived islets (SC-islets) were dissociated with TrypLE for
551 10 min at 37 °C and resuspended in 5% FBS-containing PBS. Fixation and permeabilization were
552 done using Cytofix/Cytoperm (BD Biosciences, catalog no. 554714) for 20 min at RT. Then,
553 samples were incubated overnight with primary antibodies at 4 °C, followed by secondary
554 antibodies for 30 min in RT in Perm/Wash buffer (BD Biosciences, catalog no. 554714)
555 supplemented with 5% FBS. The cells were run on FACSCalibur cytometer (BD Biosciences); data
556 were collected with CellQuest Pro v.4.0.2 (BD Biosciences) and analyzed with FlowJo™ v10.8
557 Software (BD Life Sciences). Antibodies are listed in Table S3.

558 For cell cycle analysis, wild type and knock out hiPSC were plated overnight on 6 well plates
559 containing E8 supplemented with ROCK inhibitor and 20 µM dTMP. Then, the media were
560 refreshed and for some plates the dTMP supplementation was stopped. Cells from individual
561 wells were collected at 0, 2, 4, 10, 16 and 24 h after dTMP withdrawal and fixed using 4% PFA in
562 in PBS. The same timepoint were collected for the supplemented plates. After fixation, samples
563 were washed and incubated 30 min with 10 µg/ml DAPI diluted in 1% Triton-X (Sigma-Aldrich) in
564 PBS. Then, they were immediately analyzed using the NovoCyte Quanteon 4025.

565

566 Insulin secretion analysis *in vitro*

567 For static analysis of insulin secretion, a total of 30 – 50 SC-islets were picked and incubated
568 for 90 min in a 12 well plate containing 2.8 mM glucose (G2.8) in Krebs-Ringer buffer (KRB) for
569 equilibration. This was followed by sequential 30 min incubations of G2.8, 16.8 mM glucose
570 (G16.8) and G2.8+30 mM KCl in KRB. After each incubation, 200 uL samples were taken for
571 further insulin secretion analysis. Once all samples were taken, the islets were collected for DNA
572 quantification. Dynamic insulin secretion test was carried out using a perifusion apparatus
573 (Brandel Suprafusion SF-06) at a 0.25 ml min–1 flow rate, sampling every 4 min. 50 SC-islets were
574 handpicked and perfused with KRB; sample collection started after 90 min of equilibration in
575 G2.8. The insulin content of secretion fractions and SC-islet lysates was analyzed with
576 enzymelinked immunosorbent assay (ELISA) (Mercodia).

577

578 Islet *in vivo* characterization

579 Animal care and experiments were approved by the National Animal Experiment Board in
580 Finland (ESAVI/9734/2021). NOD-SCID-Gamma (NSG, Jackson Laboratories, catalog no. 0055577)
581 mice were housed in the Biomedicum Helsinki conventional facility in 12 h light/dark cycle and
582 fed standard chow. SC-islet implantations were done following a previously stablished described
583 protocol (*4*). Non-fasted blood samples were collected monthly from the saphenous vein for
584 glucose measurement and C-peptide secretion analysis. For further characterization of the SC-
585 islet graft, the engrafted kidney was removed after 1 or 3 months and processed as described
586 below.

587 For the insulin tolerance test at 3-months post-implantation, the mice were weighted and
588 injected with insulin (0.75 IU/kg). Blood glucose was measured every 15 min for 1 hour and
589 serum samples for human C-peptide secretion analysis were at 30 and 60 min.

590

591 Hematoxylin-eosin staining

592 Teratoma-like growths were fixed using 4% PFA-PBS overnight and then embedded in paraffin
593 and sectioned.

594 Dried sections were deparaffinized and stained using a standard protocol. Briefly, they were
595 deparaffinized using xylene (3 x 10 min) and gradually hydrated using decreasing concentrations

596 of ethanol (99% EtOH 3 x 4 min, 96% EtOH 1 x 4 min, 70% EtOH 1 x 2 min). Then incubated in
597 hematoxylin for 2.5 – 3 min, washed in indirect flowing tap water for 5 - 10 min followed by a 1
598 min incubation in MQ water. The sample were incubated in eosin for 2 min and dehydrated using
599 increasing concentrations of ethanol (96% EtOH 3 x 10 sec, 99% EtOH 2 x 2 min) and xylene (2 x
600 4min). Slides were mounted with coverslips using mounting media and image the next day.
601
602 Immunocytochemistry, immunohistochemistry, and image analysis
603 Samples from hiPSC were fixed using 4%PFA-PBS for 20 min and permeabilized using 1%
604 Triton-X in PBS. Samples from S4 and S7 SC-islets were fixed with 4% PFA in PBS for 2 h, and
605 explanted SC-islet grafts and teratoma-like growths were fixed overnight. After fixation, these
606 samples were embedded in paraffin and sectioned.
607 For immunohistochemistry and immunocytochemistry, 5 µm sections were deparaffinized
608 and subjected to HIER in 0.1 mmol l–1 citrate buffer. The cells and tissue slides were blocked with
609 UV-block (Thermo Scientific, catalog no. TA-125-PBQ), and incubated with primary antibodies in
610 0.1% Tween-20 overnight at 4 °C with the given dilutions (Table S3). After washing, secondary
611 antibodies diluted in a similar manner were incubated at RT for 1 h. For immunocytochemistry,
612 secondary antibody incubation was done in the presence of Hoechst33342 for nuclear staining.
613 For immunohistochemistry, after the secondary antibody the slides were incubated with a DAB
614 solution for 2-10 min until a brown color developed. Then, they were counterstained with
615 hematoxylin for 2.5-3 min and dehydrated following a standard protocol (see hematoxylin-eosin
616 staining).
617 The cells and immunocytochemistry slides were imaged using Apotome II from a Zeiss
618 AxioImager with the same exposure and export setting used on all slides of each targeted marker.
619 Immunohistochemisty slides were imaged using an Olympus BX51 Microscope.
620 Images were processed in Zen2 Blue Edition v.2 (Zeiss) and analyzed using FiJi (*29*) or
621 CellProfiler v.4.0 (*30*) with pipelines adapted from a previous report (*31*). The same pipeline
622 settings were used on all images of each targeted marker.
623
624 Protein expression analysis

625 mRNA expression levels were analyzed by qPCR (Table S4-6). TYMS protein expression was
626 assessed by standard Western blot. Briefly, protein was extracted by using RIPA lysis buffer
627 (20-188, Millipore) supplemented with cOmplete Mini protease and phosphatase inhibitors
628 tablets (Roche). Samples were sonicated (30 sec, %50 duty cycle pulse) and centrifuged for
629 soluble protein extraction. Protein quantification was done using a Pierce BCA protein assay kit
630 (ThermoFisher) and 20-30 µg total protein were run in Mini-PROTEAN TGX Precast gels
631 (#4561033, Bio-Rad). Transfer to a nitrocellulose membrane was done using 25 V for 6 min in
632 the iBlot2 Gel Transfer device (IB21001, ThermoFisher). Then, the membrane was probed with
633 a rabbit polyclonal primary antibody against TYMS (1:2500, Proteintech; Table S3). For
634 detection, we used an anti-rabbit HRP-coupled secondary antibody (1:5000, Cell Signalling) and
635 Western ECL substrate (#1705061, Bio-Rad. As a loading control, we probed the membrane
636 with a b-actin-HRP coupled antibody (sc-47778, Santa Cruz).
637

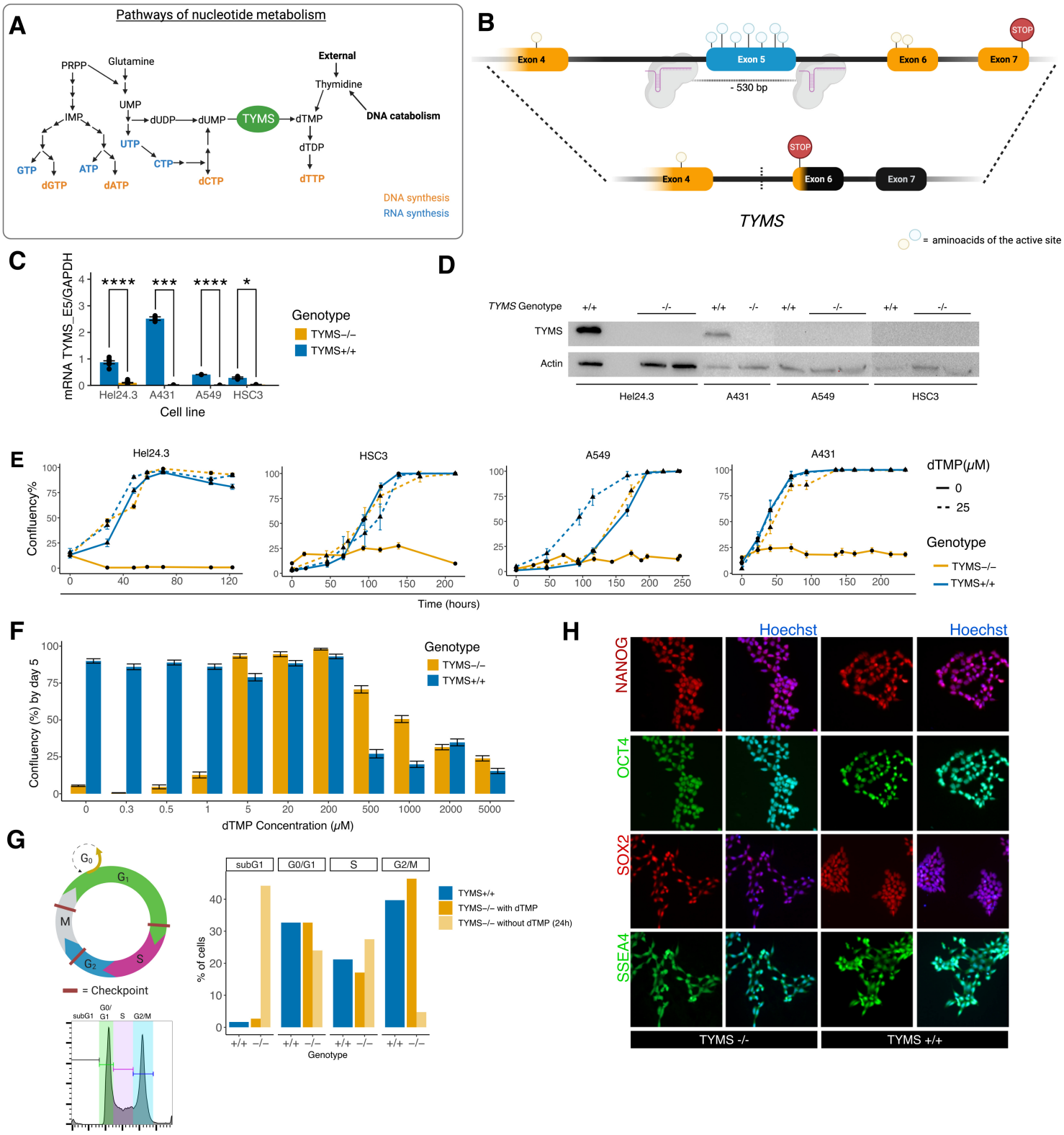
A
Pathways of nucleotide metabolism
PRPP
Glutamine
UMP
IMP
dUDP
dUMP
TYMS
dTMP
External
Thymidine
DNA catabolism
UTP
CTP
dTDP
GTP
ATP
dGTP
dATP
dCTP
dTTP
DNA synthesis
RNA synthesis
B
Exon 4
Exon 5
Exon 6
Exon 7
STOP
- 530 bp
TYMS
= aminoacids of the active site
C
mRNA TYMS_E5/GAPDH
Genotype
TYMS−/−
TYMS+/+
Hel24.3
A431
A549
HSC3
Cell line
D
TYMS Genotype
TYMS
Actin
E
Confluency%
Time (hours)
dTMP(μM)
0
25
F
Confluency (%) by day 5
dTMP Concentration (μM)
G
G0
G1
S
G2
M
= Checkpoint
subG1
G0/G1
S
G2/M
% of cells
Genotype
TYMS+/+
TYMS−/− with dTMP
TYMS−/− without dTMP (24h)
H
Hoechst
NANOG
OCT4
SOX2
SSEA4
TYMS -/-
TYMS +/+

Figure 1. A. Diagram showing the nucleotide pathways for DNA (orange) or RNA (blue) synthesis. **B.** Schematic representation of the gene of interest (*TYMS*), showing the two gRNAs, and the amino acids that form the active site of the protein over the corresponding exon that code for them. The lower line represents the change of frame upon DNA repair. **C.** TYMS expression in wild-type versus knock-out hiPSC (HEL24.3), A431, A549 and HSC3 (n=3/cell line). Results shown as ratio of *TYMS* mRNA (primer targeting exon 5) over *GAPDH* mRNA contents. **D.** Western blot showing the absence of TYMS upon inactivation of its gene. **E.** Growth curve of wild-type and knock-out cells supplemented with 0 or 25 μM dTMP. Results shown as average confluency ± SE. **F.** Confluency at day 5 of wild-type and knock-out hiPSC under different concentrations of dTMP (0 to 5000 μM). Results shown as average confluency per image ± SE. **G.** hiPSC immunocytochemistry analysis of pluripotency markers NANOG, OCT4, SOX2 and SSEA4, alone or merged with a nuclear dye channel (Hoechst). **H.** Summary of flow cyctometry results for cell cycle analysis.

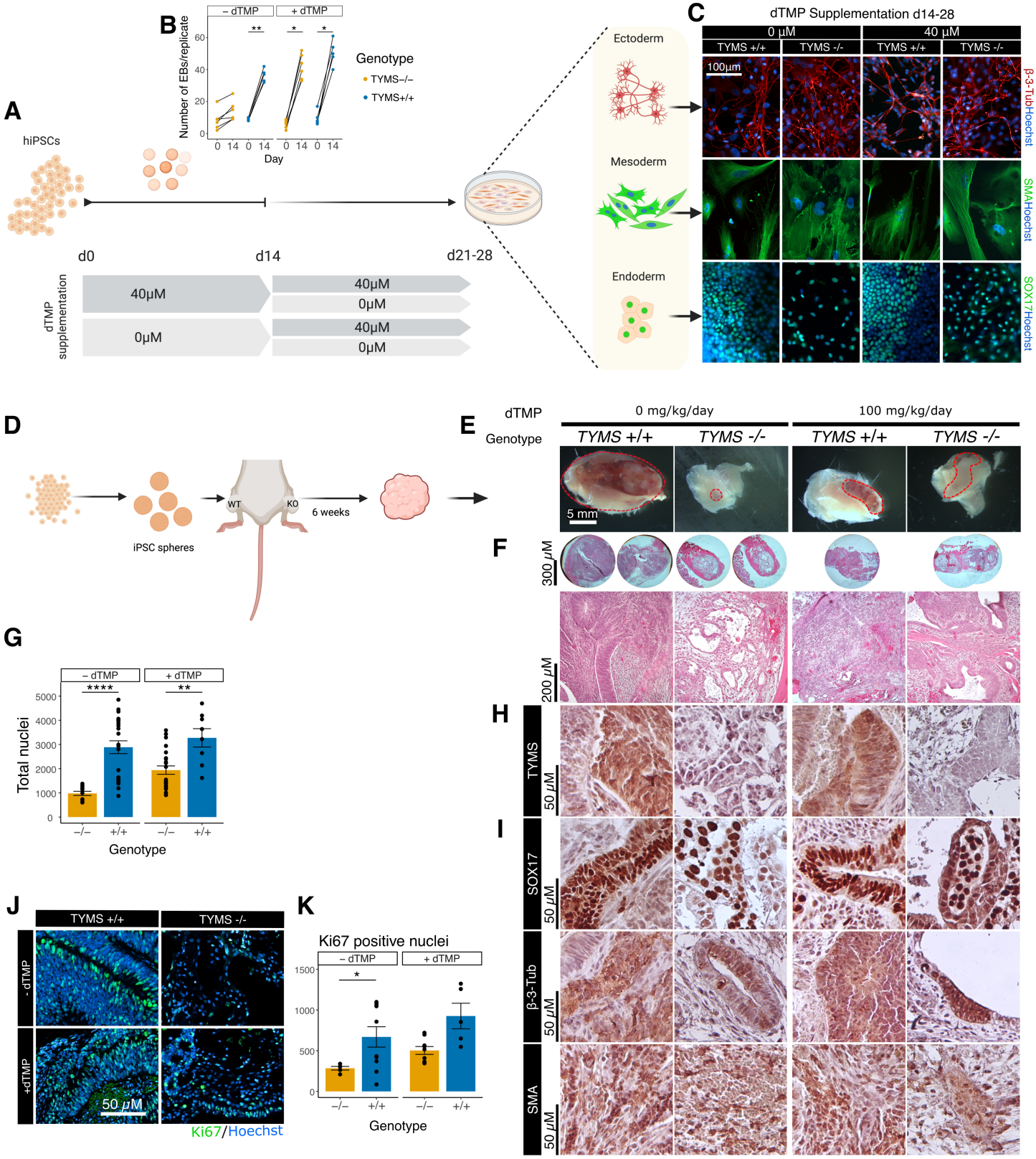
A
hiPSCs
d0
d14
d21-28
dTMP supplementation
40μM
0μM
40μM
0μM
40μM
0μM
B
– dTMP
+ dTMP
Number of EBs/replicate
Day
Genotype
TYMS−/−
TYMS+/+
C
dTMP Supplementation d14-28
0 μM
40 μM
TYMS +/+
TYMS -/-
100μm
Ectoderm
Mesoderm
Endoderm
β-3-TubHoechst
SMAHoechst
SOX17Hoechst
D
iPSC spheres
WT
KO
6 weeks
E
dTMP
Genotype
0 mg/kg/day
100 mg/kg/day
TYMS +/+
TYMS -/-
5 mm
F
300 μM
200 μM
G
– dTMP
+ dTMP
Total nuclei
Genotype
H
TYMS
50 μM
I
SOX17
β-3-Tub
SMA
J
TYMS +/+
TYMS -/-
- dTMP
+dTMP
50 μM
Ki67/Hoechst
K
Ki67 positive nuclei
– dTMP
+ dTMP
Genotype

Figure 2. A. Graphical representation of trilineage differentiation protocol. **B.** Number of resulting 300 μm aggregates from wild-type and knock-out hiPSC with and without supplementation during the first stage of differentiation (day 0 to 14). **C.** Immunocytochemisty analysis of markers for ectoderm (beta-3-tubulin) , mesoderm (smooth muscle actin, SMA), and endoderm (SOX17) in cells derived from wild-type and knock-out hiPSC under dTMP supplementation during the first stage of differentiation. **D.** Graphical representation of teratoma formation experiment. **E.** Knock-out and wild-type hiPSC-derived teratomas with and without dTMP supplementation as extracted from the mice, before processing for molecular analysis. **F.** Macro and micro images of haematoxylin-eosin staining show dense and cystic structures within the tumors. **G.** Quantification of cellularity (cell density), based on nuclear count of sectioned teratomas. **H.** Immunohistochemistry against TYMS. **I.** Immunohistochemistry of characteristic markers of endoderm (SOX17), ectoderm (beta-3-tubulin) and mesoderm (SMA). **J.** Immunohistochemistry against KI67 (proliferation marker, green) and total nuclei (Hoechst, blue). **K.** Quantification of KI67 positive nuclei from immunohistochemistry. Statistical significance in panels B, G and K based on Wilcoxon test; $p>0.05$ (ns, not shown), $p < 0.05$ (*), $p < 0.01$ (**), $p < 0.001$ (***), $p < 0.0001$ (****).

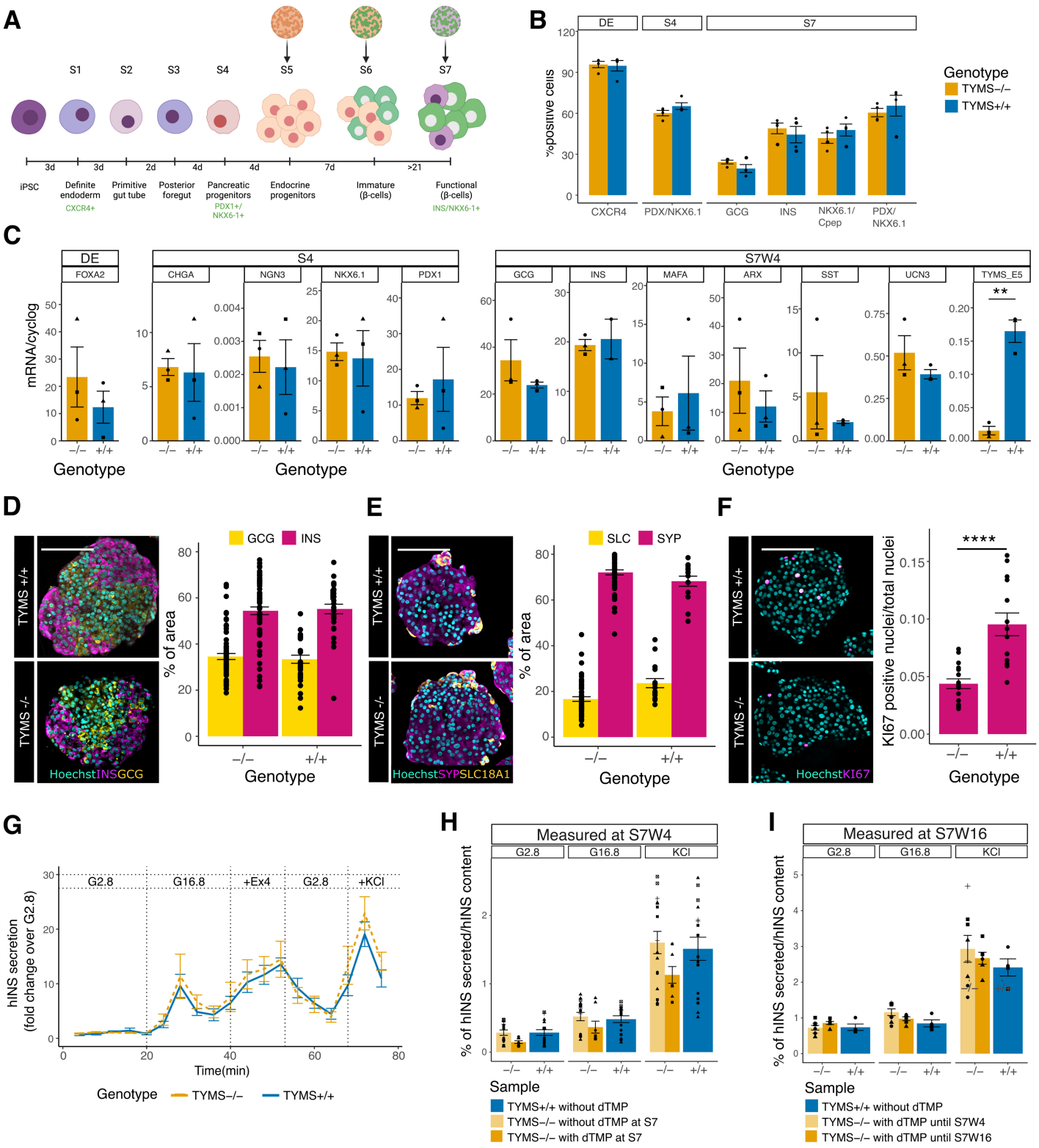
A
S1
S2
S3
S4
S5
S6
S7
3d
3d
2d
4d
4d
7d
>21
iPSC
Definite endoderm
CXCR4+
Primitive gut tube
Posterior foregut
Pancreatic progenitors
PDX1+/ NKX6-1+
Endocrine progenitors
Immature (β-cells)
Functional (β-cells)
INS/NKX6-1+
B
DE
S4
S7
%positive cells
CXCR4
PDX/NKX6.1
GCG
INS
NKX6.1/ Cpep
PDX/ NKX6.1
Genotype
TYMS−/−
TYMS+/+
C
DE
S4
S7W4
FOXA2
CHGA
NGN3
NKX6.1
PDX1
GCG
INS
MAFA
ARX
SST
UCN3
TYMS_E5
mRNA/cyclog
Genotype
D
TYMS +/+
TYMS -/-
HoechstINSGCG
GCG
INS
% of area
Genotype
E
TYMS +/+
TYMS -/-
HoechstSYPSLC18A1
SLC
SYP
% of area
Genotype
F
TYMS +/+
TYMS -/-
HoechstKI67
KI67 positive nuclei/total nuclei
Genotype
G
G2.8
G16.8
+Ex4
G2.8
+KCl
hINS secretion (fold change over G2.8)
Time(min)
Genotype
TYMS−/−
TYMS+/+
H
Measured at S7W4
G2.8
G16.8
KCl
% of hINS secreted/hINS content
Sample
TYMS+/+ without dTMP
TYMS−/− without dTMP at S7
TYMS−/− with dTMP at S7
I
Measured at S7W16
G2.8
G16.8
KCl
% of hINS secreted/hINS content
Sample
TYMS+/+ without dTMP
TYMS−/− with dTMP until S7W4
TYMS−/− with dTMP until S7W16

Figure 3. A. Graphical representation of in vitro beta cell differentiation from hiPSC. Most tests were carried out four weeks from stage 7 (S7W4), after four weeks from dTMP withdrawal. **B.** Flow cytometry analysis for markers for different stages of differentiation: CXCR4 for definite endoderm (DE) stage; NKX6.1 and PDX1 for stage 4 (S4); NKX6.1, C-peptide, PDX1, insulin (INS) and glucagon (GCG) for S7. **C.** mRNA expression analysis of maturation markers at different stages and of *TYMS* at S7 (primers target exon 5). Results are shown as ratio of marker mRNA over *GAPDH* mRNA. **D.** Immunohistochemistry and quantification of INS (magenta) and GCG (yellow) in hiPSC-derive islets at S7W4. **E**. Immunohistochemistry and quantification of synaptophysin (SYP, magenta) and SLC18A1 (yellow) in hiPSC-derive islets at S7W4. **F**. Immunohistochemistry of KI67 (magenta) in hiPSC-derive islets at S7W4 and quantification of proliferation index, as number of KI67 positive nuclei over the total nuclei. **G.** Dynamic insulin secretion in response to different stimuli at S7W4. **H-I.** In vitro insulin secretion in response to low (2.8) and high (16.8) glucose concentration and glucose plus KCl (2.8 KCl) at S7W4 (E) and S7W16 (F). Statistical significance based on Wilcoxon test; $p>0.05$ (ns, not shown), $p < 0.05$ (*), $p < 0.01$ (**), $p < 0.0001$ (****). Scalebar = 100 μM.

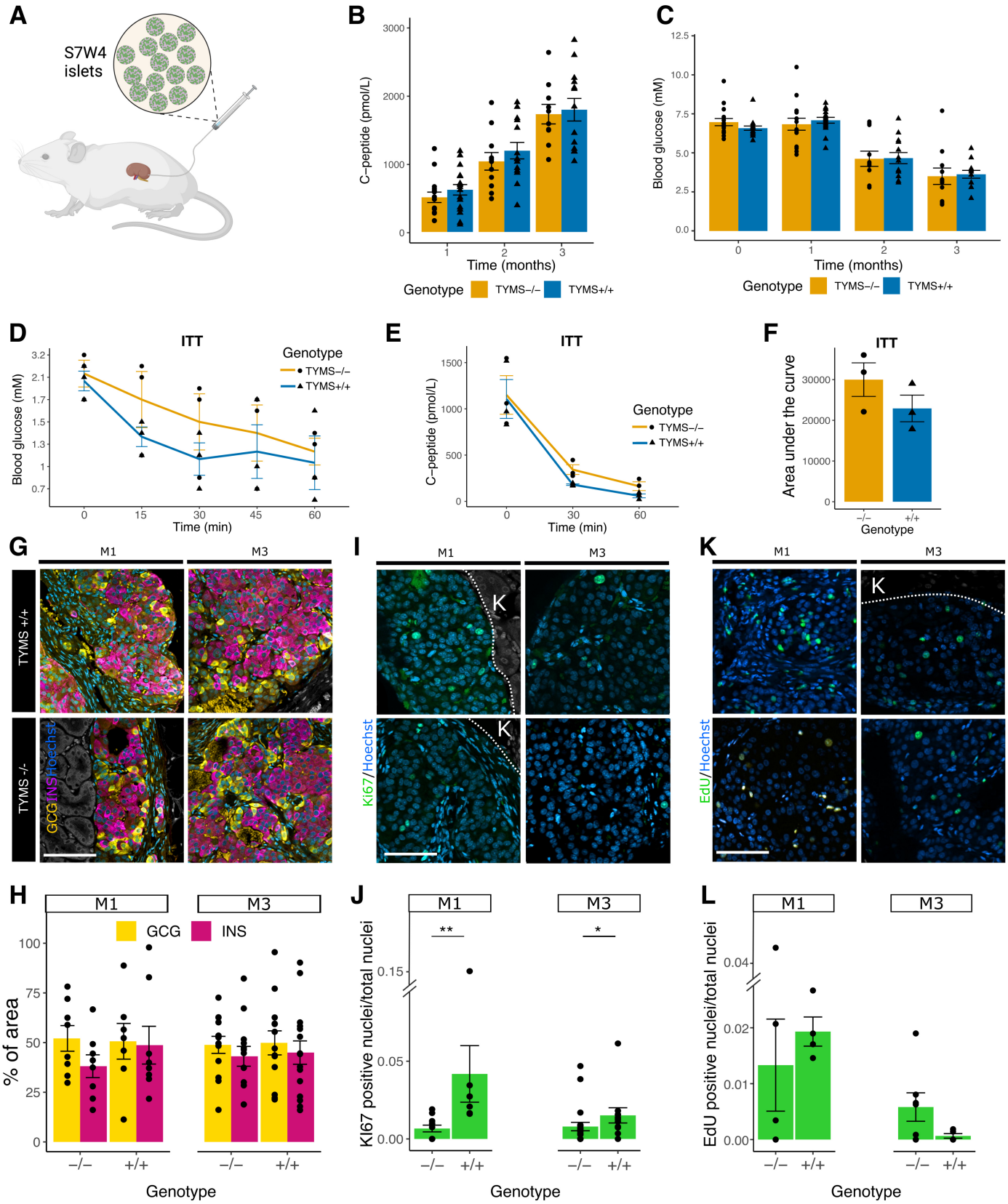
A
S7W4 islets
B
C-peptide (pmol/L)
Time (months)
Genotype
TYMS−/−
TYMS+/+
C
Blood glucose (mM)
Time (months)
Genotype
TYMS−/−
TYMS+/+
D
ITT
Blood glucose (mM)
Time (min)
Genotype
TYMS−/−
TYMS+/+
E
ITT
C-peptide (pmol/L)
Time (min)
Genotype
TYMS−/−
TYMS+/+
F
ITT
Area under the curve
Genotype
G
M1
M3
TYMS +/+
TYMS -/-
GCG/INS/Hoechst
I
M1
M3
K
Ki67/Hoechst
K
K
M1
M3
K
EdU/Hoechst
H
M1
M3
GCG
INS
% of area
Genotype
J
M1
M3
Ki67 positive nuclei/total nuclei
Genotype
L
M1
M3
EdU positive nuclei/total nuclei
Genotype

Figure 4. A. Diagram of S7W4 islet implantation set-up. **B-C**. Follow up of human C-peptide secretion (in serum), and blood glucose in mice after 1-, 2- and 3-months from implantation (month 0). **D**. Blood glucose of mice under ITT at every 15 min for 1 hour. **E**. Human C-peptide secretion (in serum) during ITT before and after 30 min and 1 hour from insulin administration. **F**. Quantification of area under the curves of human-C-peptide secretion. **G**. Immunohistochemistry of engrafted kidney 1- and 3-months post-implantation. INS (magenta), GCG (yellow). **H**. Quantification of INS and GCG area in the islets from G. **I**. Immunohistochemistry against KI67 in grafts after 1 and 3 months. **J**. Proliferation index, based on the quantification of KI67 positive nuclei over the total number of nuclei from I. **K**. Immunohistochemistry against EdU in grafts after 1 and 3 months. **L**. Quantification of EdU positive nuclei over the total number of nuclei from K. Statistical significance based on Wilcoxon test; $p>0.05$ (ns, not shown) $p < 0.05$ (*), $p < 0.01$ (**). K = kidney. Scalebar = 50 μM.

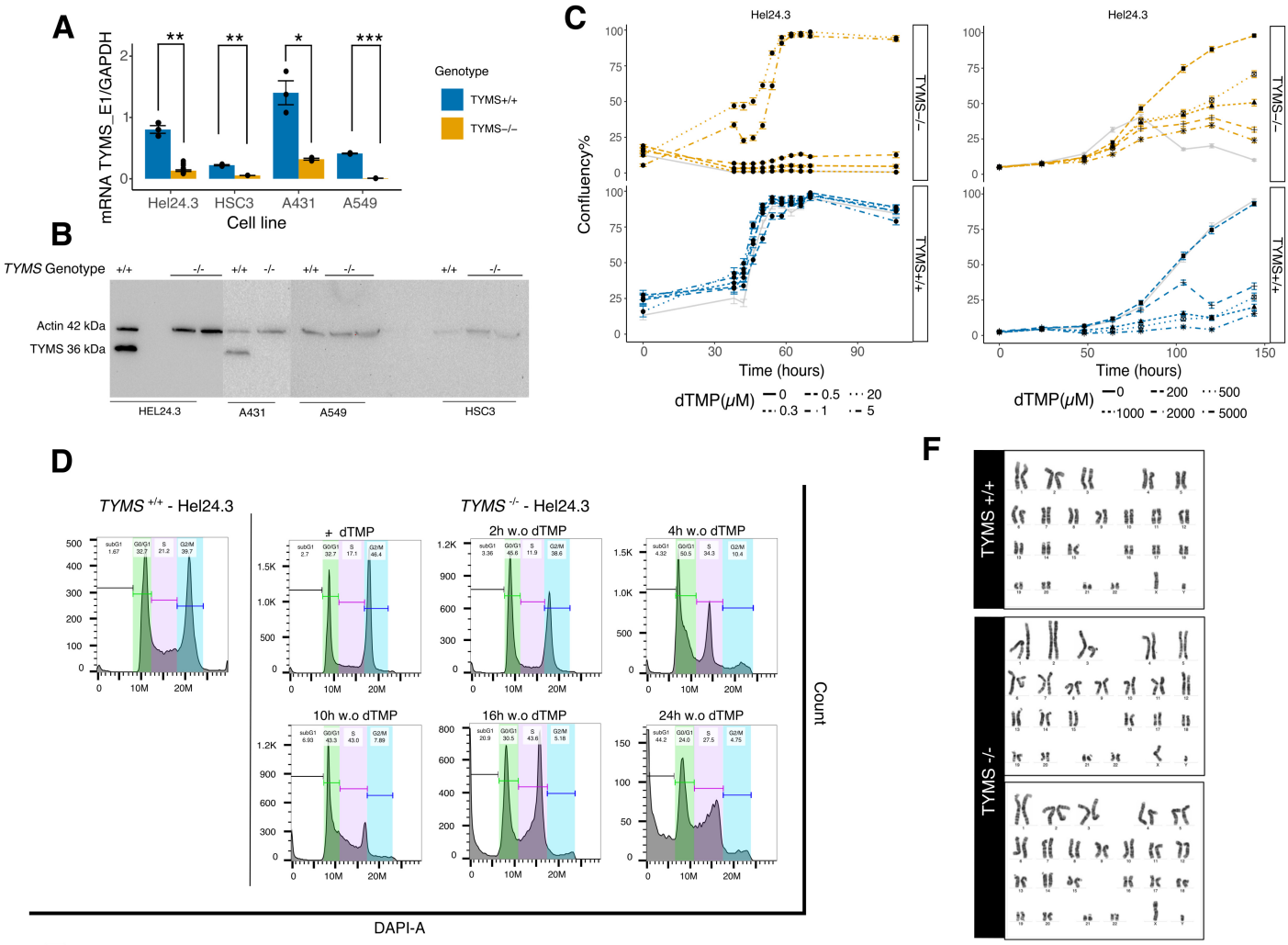

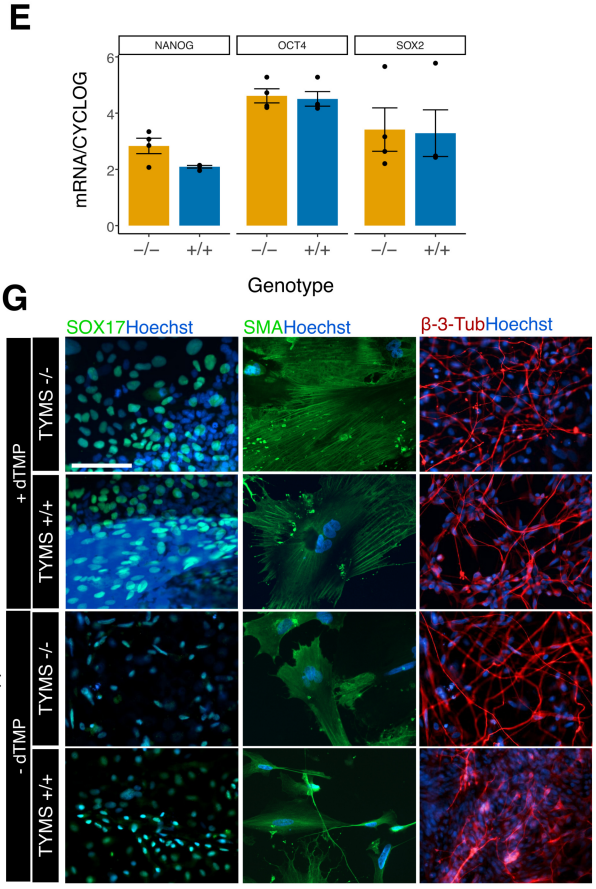

Supplementary figure 1. A. *TYMS* mRNA expression in wild-type versus knock-out cell lines (HEL24.3, A431, A549 and HSC3) using primers targeting exon 1 (n=3/cell line). Results shown as ratio of *TYMS* mRNA over *GAPDH* mRNA. **B**. Full western blot membranes of TYMS in wild-type and edited cell lines. **C**. Full growth curves of wild-type and knock-out hiPSC under different concentrations of dTMP (0 to 5000 μM). Results shown as average confluency per image ± SD. **D**. Cell cycle analysis of knock-out hiPSC during the first 24h after dTMP withdrawal. **E**. Karyotype of wild-type hiPSC, passage 20. Karyotype of TYMS-knock-out hiPSC, passage 20 (up) and passage 45 (down). **F**. hiPSC RT-qPCR for expression analysis of pluripotency markers *NANOG, OCT4* and *SOX2*. Results shown as ratio of mRNA over *CYCLOG* mRNA. **G**. Immunocytochemistry against markers for endoderm (SOX17), mesoderm (SMA), and ectoderm (beta-3-tubulin) in cells derived from wild-type and knock-out hiPSC without dTMP supplementation during the first stage of differentiation. Statistical significance in panel A and F based on Wilcoxon test; $p < 0.05$ (*), $p < 0.01$ (**), $p < 0.001$. Scalebar = 100 μM.

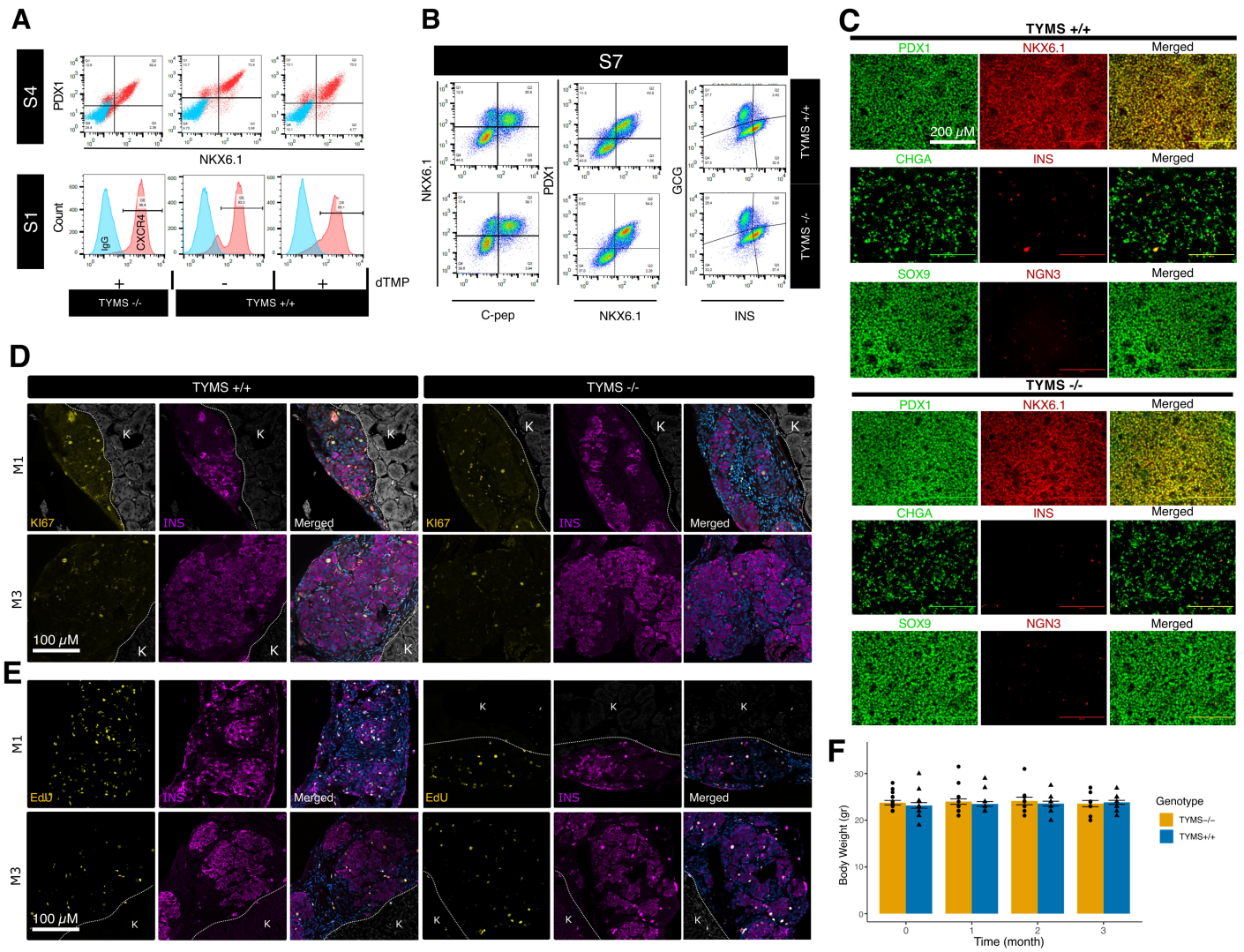

Supplementary figure 2. A. Flow cytometry analysis of characteristic markers for definite endoderm (CXCR4) and stage 4 (NKX6.1 and PDX1) of beta-cell differentiation protocol. **B**. Flow cytometry analysis of markers at stage 7 of beta-cell differentiation: NKX6.1, C-peptide, PDX1, insulin (INS) and glucagon (GCG). **C**. Immunocytochemistry analysis of maturation markers at S4 of beta-cell differentiation protocol. First row: PDX1 and NKX6.1. Second row: CHGA and INS. Third row: SOX9 and NGN3. **D-E**. Immunocytochemistry against KI67 (yellow, D) and EdU (yellow, E) on insulin positive cells (magenta) from beta-cell grafts at 1 or 3 months after implantation under the kidney capsule (M1 and M3, respectively). **F**. Body weight of mice after 1-, 2- and 3-months from implantation (month 0). K = kidney